Letter

Polynomial sign problem and topological Mott insulator in twisted bilayer graphene

Xu Zhang [1], Gaopei Pan [2,3], Bin-Bin Chen [1], Heqiu Li [4], Kai Sun [5,*] and Zi Yang Meng [1,†]

[1] *Department of Physics and HKU-UCAS Joint Institute of Theoretical and Computational Physics, The University of Hong Kong, Pokfulam Road, Hong Kong SAR, China*

[2] *Beijing National Laboratory for Condensed Matter Physics and Institute of Physics, Chinese Academy of Sciences, Beijing 100190, China*

[3] *School of Physical Sciences, University of Chinese Academy of Sciences, Beijing 100049, China*

[4] *Department of Physics, University of Toronto, Toronto, Ontario M5S 1A7, Canada*

[5] *Department of Physics, University of Michigan, Ann Arbor, Michigan 48109, USA*

(Received 22 October 2022; accepted 8 June 2023; published 20 June 2023)

We show that for the magic-angle twisted bilayer graphene (TBG) away from the charge neutrality point, although quantum Monte Carlo (QMC) simulations suffer from the sign problem, the computational complexity is at most polynomial at integer fillings of the flat-band limit. For even-integer fillings, the polynomial complexity survives even if an extra intervalley attractive interaction is introduced. This observation allows us to simulate magic-angle TBG and to obtain an accurate phase diagram and dynamical properties. At the chiral limit and filling $\nu = 1$, the simulations reveal a thermodynamic transition separating the metallic state and a $C = 1$ correlated Chern insulator—topological Mott insulator (TMI)—and the pseudogap spectrum slightly above the transition temperature. The ground state excitation spectra of the TMI exhibit a spin-valley U(4) Goldstone mode and a time-reversal restoring excitonic gap smaller than the single-particle gap. These results are qualitatively consistent with recent experimental findings at zero-field and $\nu = 1$ filling in *h*-BN nonaligned TBG devices.

DOI: 10.1103/PhysRevB.107.L241105

Introduction. Magic-angle twisted bilayer graphene (TBG) has attracted great attention in recent years, as it hosts a variety of nontrivial phases beyond semiclassical or band-theory description [1–41]. To theoretically characterize these flat bands and correlated quantum phases, tight-binding [2,5] and continuous Bistritzer-MacDonald (BM) [3] models have been developed. In this Letter, we focus on the continuous-model approach, which avoids the challenge to construct localized orbitals that preserve all the symmetries [34,42–46]. By projecting long-range Coulomb interactions onto the moiré flat bands with a quantum metric, such a projected Hamiltonian has been studied using mean-field approximations [20,31,47,48]. At certain limits, an exact analytical solution has also been obtained [49–53]. On the numerical side, the charge neutrality point has been studied using sign-problem-free momentum-space quantum Monte Carlo (QMC) simulations [54–56]. However, away from the charge neutrality point, due to the emerging sign problem, such simulations have not yet been performed.

Although the sign problem often implies exponential computational complexity, it is worthwhile to emphasize that not all sign problems cause such severe damage. Very recently, a much milder type of sign problem has been demonstrated, where the computational complexity scales as a polynomial function of the system size, known as the polynomial sign problem [57–59].

In this Letter, we study the sign problem in TBG at the flat-band limit (the interaction effect will be overestimated which will cause a quantitative difference for a gapped insulator ground state). Utilizing the sign bound theory [58], we prove that TBG flat bands at even-integer fillings, or arbitrary integer fillings in the chiral limit, exhibit (at most) a polynomial sign problem. This observation allows us to utilize QMC methods to study TBG systems with fillings away from charge neutrality, away from the chiral limit, and/or in the presence of extra attractive interactions with phononic or topological origins [18,21,60,61] on top of the Coulomb repulsion.

To demonstrate this approach, we performed large-scale QMC simulations to examine the chiral limit at filling $\nu = 1$ (we denote the fully empty/filled flat bands as $\nu = -4/+4$ and charge neutrality as $\nu = 0$). At $T = 0$, this model can be solved exactly [50,52,55], and the exact solution reveals that at $T \to 0$, the system is a correlated Chern insulator—a topological Mott insulator (TMI) [62–67]—with a Chern number $C = 1$. Upon raising the temperature, our QMC simulations observe three different phases/states: (1) a metal phase with time-reversal symmetry at high temperature $T > T^\star$, (2) a time-reversal invariant pseudogap phase at intermediate temperature $T_c < T < T^\star$, and (3) a low-temperature TMI phase at $T < T_c$. Here, $T^\star$ is a crossover temperature scale and T_c is the critical temperature below which the time-reversal symmetry is spontaneously broken. We further show that in the TMI phase spins remain disordered due to thermal excitations of gapless spin fluctuations. This absence of spin order/polarization is in direct contrast to quantum Hall systems where electron spins are polarized due to Zeeman splitting and thus spin fluctuations are gapped.

*sunkai@umich.edu
†zymeng@hku.hk

BM model and projected interaction. We utilize the BM model and project interactions between fermions to the moiré flat bands. The BM model Hamiltonian [3] for the τ valley takes the following form,

$$H^{\tau}_{\mathbf{k},\mathbf{k}'} = \begin{pmatrix} \hbar v_F(\mathbf{k}-\mathbf{K}_1)\cdot\boldsymbol{\sigma}\delta_{\mathbf{k},\mathbf{k}'} & V \\ V^{\dagger} & \hbar v_F(\mathbf{k}-\mathbf{K}_2)\cdot\boldsymbol{\sigma}\delta_{\mathbf{k},\mathbf{k}'} \end{pmatrix}, \tag{1}$$

where $\mathbf{K}_1$ and $\mathbf{K}_2$ mark the two Dirac points in the τ valley from layers 1 and 2, respectively. $V = U_0\delta_{\mathbf{k},\mathbf{k}'} + U_1\delta_{\mathbf{k},\mathbf{k}'-\mathbf{G}_1} + U_2\delta_{\mathbf{k},\mathbf{k}'-\mathbf{G}_1-\mathbf{G}_2}$ and $V^{\dagger} = U_0^{\dagger}\delta_{\mathbf{k},\mathbf{k}'} + U_1^{\dagger}\delta_{\mathbf{k},\mathbf{k}'+\mathbf{G}_1} + U_2^{\dagger}\delta_{\mathbf{k},\mathbf{k}'+\mathbf{G}_1+\mathbf{G}_2}$ are the interlayer tunnelings with matrix

$$U_n = \begin{pmatrix} u_0 & u_1 e^{-i\frac{2\pi}{3}n} \\ u_1 e^{i\frac{2\pi}{3}n} & u_0 \end{pmatrix}, \tag{2}$$

where u_0 and u_1 are the intra- and intersublattice interlayer tunneling amplitudes. $\mathbf{G}_1 = (-1/2, -\sqrt{3}/2)$, $\mathbf{G}_2 = (1, 0)$ are the reciprocal vectors of the moiré Brillouin zone (mBZ), and $\mathbf{K}_1 = (0, 1/2\sqrt{3})|\mathbf{G}_{1,2}|$, $\mathbf{K}_2 = (0, -1/2\sqrt{3})|\mathbf{G}_{1,2}|$. For parameters, we set $(\theta, \hbar v_F/a_0, u_0, u_1) = (1.08^{\circ}, 2.377\,45\ \text{eV}, 0\ \text{eV}, 0.11\ \text{eV})$ for the chiral limit, and for nonchiral model, we set $u_0 = 0.06$ eV following Refs. [49,54,56,68]. Here, θ is the twisting angle and a_0 is the lattice constant of monolayer graphene.

For interactions, in addition to the Coulomb repulsion, here we have the option to include one more interaction term and the sign problem will still remain polynomial:

$$\begin{aligned} H_I &= \frac{1}{2\Omega}\sum_{\mathbf{q}}[V_1(\mathbf{q})\delta\rho_{1,\mathbf{q}}\delta\rho_{1,-\mathbf{q}} + V_2(\mathbf{q})\delta\rho_{2,\mathbf{q}}\delta\rho_{2,-\mathbf{q}}], \\ \delta\rho_{1,\mathbf{q}} &= \sum_{\mathbf{k},\alpha,\tau,s}\left(c^{\dagger}_{\mathbf{k},\alpha,\tau,s}c_{\mathbf{k}+\mathbf{q},\alpha,\tau,s} - \frac{\nu+4}{8}\delta_{\mathbf{q},0}\right), \\ \delta\rho_{2,\mathbf{q}} &= \sum_{\mathbf{k},\alpha,s}(c^{\dagger}_{\mathbf{k},\alpha,\tau,s}c_{\mathbf{k}+\mathbf{q},\alpha,\tau,s} - c^{\dagger}_{\mathbf{k},\alpha,-\tau,s}c_{\mathbf{k}+\mathbf{q},\alpha,-\tau,s}). \end{aligned} \tag{3}$$

The first term in H_I ($V_1 > 0$) is the Coulomb interactions, and the second term $V_2 \geqslant 0$ introduces repulsive interactions for fermions in the same valley and attractions between the two valleys, which is a phenomenological term describing intervalley attractions [18,21,60,61,69–73]. At $V_2 = 0$, this model recovers the standard TBG model with Coulomb repulsion. When V_2 is turned on, the intervalley attraction favors intervalley pairing and could stabilize a superconducting ground state. The normalization factor in H_I is $\Omega = L^2\frac{\sqrt{3}}{2}a_M^2$ with L and a_M being the linear system size of the system and the moiré unit cell length. $\mathbf{k}$ and $\mathbf{q}$ cover the whole momentum space, ν is the filling factor, and α, τ, s represent the layer/sublattice, valley, and spin indices, respectively. The momentum dependence for non-negative V_1 and V_2 is unimportant to the polynomial sign problem. Here, for simplicity, we set $V_2 = \gamma V_1$ with γ being a non-negative constant and for V_1, we use a Coulomb interaction screened by a single gate $V_1(\mathbf{q}) = \frac{e^2}{4\pi\varepsilon}\int d^2\mathbf{r}(\frac{1}{\mathbf{r}} - \frac{1}{\sqrt{\mathbf{r}^2+d^2}})e^{i\mathbf{q}\cdot\mathbf{r}} = \frac{e^2}{2\varepsilon}\frac{1}{|\mathbf{q}|}(1-e^{-|\mathbf{q}|d})$, where $\frac{d}{2} = 20$ nm is the distance between the graphene layer and single gate, and $\epsilon = 7\epsilon_0$ is the dielectric constant. We then project the interactions H_I to the moiré flat bands [see Supplemental Material (SM) [74]] and use the projected Hamiltonian to carry out a sign bound analysis and QMC simulations.

Polynomial sign bounds. In the QMC simulations, the expectation value of a physical observable $\hat{O}$ is measured as $\langle\hat{O}\rangle = \sum_l W_l\langle\hat{O}\rangle_l$, where W_l and $\langle\hat{O}\rangle_l$ are the weight and the expectation value for the configuration l [74,75]. In sign-problem-free QMC simulations, $W_l \geqslant 0$ for all l and an accurate expectation value can be obtained by only sampling a small number of configurations, the importance sampling, and this number scales as a power-law function of the system size. However, for many quantum systems, W_l can be negative or even complex, and thus to obtain an accurate expectation value, it requires sampling a large number of configurations, which usually scales as an exponential function of the system size [75,76].

It is worthwhile to emphasize that the sign problem does not always lead to an exponentially high computational cost. The average sign $\langle\text{sign}\rangle = \sum_l W_l/\sum_l|\text{Re}(W_l)|$ between 0 and 1 is usually used to measure the severity of the sign problem. $\langle\text{sign}\rangle = 1$ means that the system is sign problem free, while smaller $\langle\text{sign}\rangle$ means a more severe sign problem. In a d-dimensional quantum system that suffers from the sign problem, $\langle\text{sign}\rangle \sim \exp(-\beta L^d)$ where $\beta = 1/T$, the inverse temperature, indicates that the number of configurations needed in QMC simulations scales as an exponential function of the space-time volume [75,76]. For a polynomial sign problem, although $\langle\text{sign}\rangle < 1$ (i.e., the system does suffer from the sign problem), $1/\langle\text{sign}\rangle$ is a polynomial function of the system size and thus the number of configurations needed only scales as a power-law function of the system size.

Although the average sign can be easily measured in QMC simulations, it usually does not have a simple analytic formula. To estimate the numerical cost of overcoming the sign problem, we utilize the sign bound $\langle\text{sign}\rangle_b$ defined in Ref. [58] in which $\langle\text{sign}\rangle_b$ is proved to be the lower bound of $\langle\text{sign}\rangle$ (i.e., $\langle\text{sign}\rangle_b \leqslant \langle\text{sign}\rangle$). Thus, if the sign bound scale is a power-law function of the system size, the sign problem is (at most) polynomial. Remarkably, the low-temperature sign bound in moiré flat bands can be easily calculated by counting the ground state degeneracy, which can be obtained using the SU(4) and SU(2) Young diagrams as employed in Refs. [49,50,55] (see SM for details [74]).

At charge neutrality ($\nu = 0$), moiré flat bands with Coulomb interactions ($\gamma = 0$) are known to be sign problem free [54,55], and thus the sign bound is 1. Here, we further prove that adding intervalley attractions ($\gamma > 0$) to the chiral system does not cause a sign problem ($\langle\text{sign}\rangle_b = 1$). Away from charge neutrality, a sign problem arises, but it is polynomial at most integer fillings. For Coulomb repulsion ($\gamma = 0$), the sign problem is polynomial at any (even) integer fillings at (away from) the chiral limit. When intervalley attractions are introduced ($\gamma > 0$), even-integer fillings at the chiral limit also have a polynomial sign bound. A finite band dispersion can be included in the QMC simulation in principle, but there is no obvious theory to promise there is no general exponential sign problem.

To further verify the polynomial sign problem summarized in Table I, we directly calculate $\langle\text{sign}\rangle$ and $\langle\text{sign}\rangle_b$ in QMC simulations at various fillings ν, and compare them with the exact formula of the sign bound obtained at integer fillings. As

TABLE I. Scaling of the sign bound $\langle \text{sign} \rangle_b$ at low temperature and large moiré lattice size $N = L^2$. A power-law function of N indicates that the sign problem is (at most) polynomial. ✗ indicates the sign bound decays to zero exponentially.

Filling (ν)	Chiral ($\gamma = 0$)	Nonchiral ($\gamma = 0$)	Chiral ($\gamma > 0$)
0	1	1	1
± 1	N^{-1}	✗	✗
± 2	N^{-2}	N^{-1}	N^{-2}
± 3	N^{-5}	✗	✗
± 4	N^{-8}	N^{-4}	N^{-4}

shown in Fig. 1, $\langle \text{sign} \rangle$ is always larger than or equal to $\langle \text{sign} \rangle_b$ as expected, and the sign bound at integer filling indeed converges to the exact solution. The peak in $\langle \text{sign} \rangle$ at integer (or even-integer) fillings indicates that the sign problem is less severe and QMC simulations have a faster convergence at these fillings, and the locations of these peaks are fully consistent with the polynomial sign problem summarized in Table I.

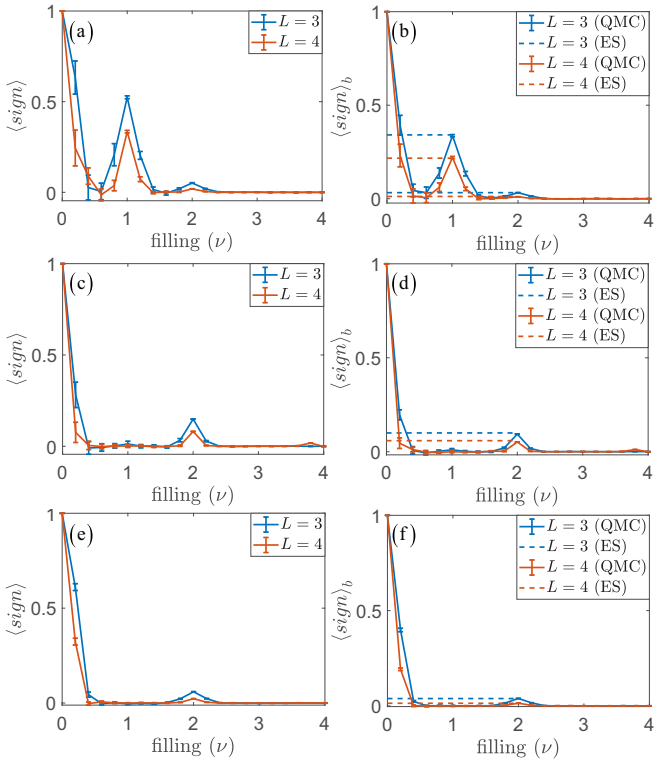

FIG. 1. (a), (c), (e) $\langle \text{sign} \rangle$ vs filling ν and (b), (d), (f) $\langle \text{sign} \rangle_b$ vs filling ν at low temperature $T = 1$ meV. The fillings of $\nu < 0$ are symmetric with respect to $\nu = 0$ via the particle-hole symmetry. (a) and (b) are the chiral limit $\gamma = 0$ cases, (c) and (d) are the nonchiral $\gamma = 0$ cases where we take $u_0 = 0.06$ eV, and (e) and (f) are the chiral limit $\gamma = 4$ cases. (a), (c), (d) are the average sign $\langle \text{sign} \rangle$ for $L = 3$ ($N = 9$) and $L = 4$ ($N = 16$) measured from QMC for filling from $\nu = 0$ to $\nu = 4$. (b), (d), (f) are the sign bounds $\langle \text{sign} \rangle_b$ for $L = 3$ ($N = 9$) and $L = 4$ ($N = 16$) measured from QMC (solid line) and derived from exact solution (ES) at the low-temperature limit for filling $\nu = 1, 2$ (dashed line values).

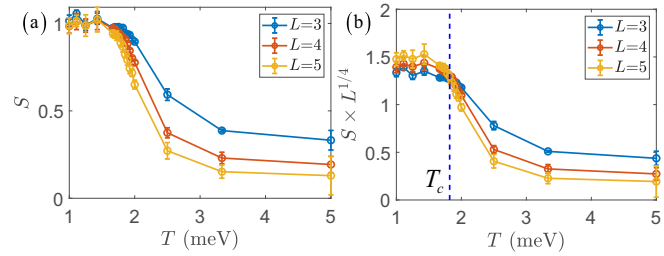

FIG. 2. (a) Chern band polarization correlation function S vs T. At low temperature, the Chern number approaches 1. (b) 2D Ising universality class crossing to determine the phase transition point at $T_c \sim 1.82 \pm 0.05$ meV, denoted by the dashed line.

Chiral limit at $\nu = 1$ and $\gamma = 0$. With the polynomial sign bound obtained, we discuss the QMC results as a function of temperature for the chiral limit $\nu = 1$ filling. In the QMC simulation, we observe a thermal phase transition with a pseudogap spectrum and spontaneous time-reversal symmetry breaking, which is of immediate relevance to the recent experimental finding of correlated Chern insulators at zero-field and $\nu = 1$ filling in h-BN nonaligned TBG devices and its relatively high Curie temperature of $T_c \sim 4.5$ K [41].

At the low-temperature limit for $\nu = 1$, an exact solution at $T = 0$ expects degenerate ground states with Chern numbers $C = \pm 1$ and ± 3 [50,52,55]. In the large system size limit $N \to \infty$, the number of ground states scales as N^7 for $C = \pm 1$ and N^3 for $C = \pm 3$ [74]. Due to the higher number of ground state degeneracies, thermal fluctuations shall stabilize the $C = \pm 1$ state as the thermal equilibrium state at low temperature via the order by disorder mechanism [77]. This low-temperature state breaks spontaneously the time-reversal symmetry, but this symmetry breaking process as a function of temperature is unknown.

Our QMC simulation at finite temperature reveals this process. To probe the time-reversal symmetry breaking, we use the Chern band polarization as the order parameter, $\langle \hat{N}_+ - \hat{N}_- \rangle / N$, where $\hat{N}_\pm$ are the fermion occupation number operators of $\pm$ Chern bands. The correlation function of this order parameter is plotted in Fig. 2, $S \equiv \langle (\hat{N}_+ - \hat{N}_-)^2 \rangle / N^2$, and a scaling analysis reveals a second-order phase transition at $T_c \sim 1.82 \pm 0.05$ meV, below which the time-reversal symmetry is spontaneously broken, similar to what was observed at $\nu = 3$ with real-space effective models [59,63,64]. At low temperature, S approaches 1, indicating that the Chern number is $C = \pm 1$, instead of ± 3. In Fig. 2(b), we rescale the data as $S \times L^{2\beta/\nu}$ using the two-dimensional (2D) Ising exponents $\beta = 1/8$ and $\nu = 1$, and the cross point at $T_c \sim 1.82 \pm 0.05$ meV marks the critical temperature. We note that our T_c is higher than the experimental results in Ref. [41], and this is because the real material is not at the chiral limit and finite u_0 would reduce the T_c [78].

Such a spontaneously generated Chern insulator is of both theoretical and experimental interest as in the temperature range of $0 < T < T_c$, it only breaks the time-reversal symmetry but not the spin-valley U(4) continuous symmetry. In contrast to quantum Hall states, where fermion spins are polarized due to Zeeman splitting, spin degrees of freedom do not form any order in this TMI phase and the spin SU(2)

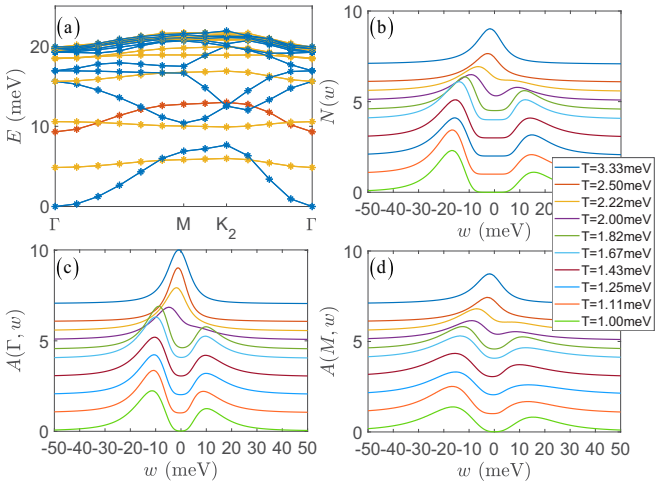

FIG. 3. (a) Analytical excitation spectra along a high-symmetry path in mBZ. The red line labels the single-particle excitations. Blue lines show the ten lowest charge-neutral excitons between bands with the same Chern number. The yellow lines label the ten lowest charge-neutral excitons between opposite Chern bands, which are responsible for the restoration of time-reversal symmetry. (b)–(d) Local density of states $N(\omega)$, and the single-particle spectra $A(\Gamma, \omega)$ and $A(M, \omega)$ obtained from the QMC-SAC scheme as a function of T. Different lines are lifted in the y direction with the amount of $\Delta\beta = \Delta(1/T)$ for clarity. Between the high-temperature metal-like phase and the low-temperature TMI phase, pseudogap behavior can be found at $T^\star \sim 2$ meV above $T_c \sim 1.82 \pm 0.05$ meV.

symmetry is preserved. To better demonstrate this point, we follow the method in Ref. [51] and analytically compute the spectrum of single-particle and charge-neutral excitonic excitations at $T = 0$. As shown in Fig. 3(a), single-particle excitations (red stars) are fully gapped, indicating an insulating state. To restore the time-reversal symmetry, it requires moving fermions from + Chern bands to − Chern bands (or vice versa). However, such particle-hole excitations are fully gapped [yellow stars in Fig. 3(a)], and thus thermal fluctuations at low T cannot restore the time-reversal symmetry. In contrast, particle-hole excitations between spin-valley bands with the same Chern number (blue starts) are gapless. These excitons describe spin-valley SU(4) fluctuations, and any spin or spin-valley order would be destroyed by these gapless excitations at any finite temperature.

We note that the energy scale of the single-particle gap is larger than the gap of time-reversal-restoring excitons [Fig. 3(a)], indicating that time-reversal symmetry breaking is probably more vulnerable to thermal fluctuations in comparison to single-particle excitations. To probe this physics, we employ the stochastic analytic continuation (SAC) method upon the QMC imaginary time data of the Green's function to extract the real-frequency single-particle spectra [54,56,72,79–91].

The obtained local density of states (LDOS) $N(\omega)$ and the single-particle spectral functions $A(\Gamma, \omega)$ and $A(M, \omega)$ are shown in Figs. 3(b)–3(d), respectively. From them, one sees that slightly above the $T_c \sim 1.82 \pm 0.05$ meV, at $T^\star = 2$ meV, the spectra indeed develop a pseudogap shape at both momenta and $N(\omega)$. Below T_c, the spectra are fully gapped and the system is an interaction-driven topological Mott insulator [62–64] with no spin polarization and Chern number $C = 1$. The pseudogap behavior at $T_c < T < T^\star$ is certainly beyond the mean-field description of the system, which would require the gap to open exactly at the transition, and is the manifestation of the intricate competition between the single-particle, collective excitations (such as the excitons), and thermal fluctuations in the moiré system. Our LDOS results at low temperature with asymmetric spectral weights are also consistent with the scanning tunneling microscopy (STM) experiment at $\nu = 1$ [11].

Discussion. The experimental observation of the zero-field Chern insulators in TBG, at $\nu = 1$ and with $C = 1$ [41], clearly poses the question that how to understand the rich physics in pristine TBG systems, but it is known that the model level computations, taking into account the strong interaction and topological ingredient of the flat-band wave functions at finite temperature, are notoriously challenging. Here, we find the way out by using the fermion sign bound theory [58], upon which we prove for Coulomb interactions and chemical potentials projected on the flat-band TBG model, that all integer fillings at chiral and even-integer fillings at nonchiral cases have either no sign problem or polynomial sign bounds in their QMC simulations. Similar behavior is also retained when a projected effective attraction is introduced for chiral even-integer fillings.

This approach allows us to unbiasedly compute the physical properties of the model at finite temperature. For $\nu = 1$, the numerical results are fully consistent with experimental observations, including spontaneous time-reversal symmetry breaking, Chern number $C = 1$, and the asymmetry in LDOS. For $T_c < T < T^\star$, the simulation reveals a pseudogap phase. This result is consistent with the observation of insulatinglike behavior at $T > T_c$ [11]. This pseudogap phase would be an interesting subject for further experimental studies, which will help us better understand the phase transition and mechanism that drives the time-reversal symmetry breaking in moiré flat bands.

Acknowledgments. We thank Wang Yao for discussions on the related topic. X.Z., G.P.P., B.-B.C., and Z.Y.M. acknowledge support from the Research Grants Council of Hong Kong SAR of China (Grants No. 17301420, No. 17301721, No. AoE/P-701/20, and No. 17309822), the ANR/RGC Joint Research Scheme sponsored by Research Grants Council of Hong Kong SAR of China and French National Research Agency (Project No. A_HKU703/22), the Strategic Priority Research Program of the Chinese Academy of Sciences (Grant No. XDB33000000), the K. C. Wong Education Foundation (Grant No. GJTD-2020-01) and the Seed Funding "Quantum-Inspired explainable-AI" at the HKU-TCL Joint Research Centre for Artificial Intelligence. We thank HPC2021 system under the Information Technology Services and the Blackbody HPC system at the Department of Physics, the University of Hong Kong for their technical support and generous allocation of CPU time.

[1] J. M. B. Lopes dos Santos, N. M. R. Peres, and A. H. Castro Neto, Phys. Rev. Lett. **99**, 256802 (2007).

[2] G. Trambly de Laissardière, D. Mayou, and L. Magaud, Nano Lett. **10**, 804 (2010).

[3] R. Bistritzer and A. H. MacDonald, Proc. Natl. Acad. Sci. USA **108**, 12233 (2011).

[4] J. M. B. Lopes dos Santos, N. M. R. Peres, and A. H. Castro Neto, Phys. Rev. B **86**, 155449 (2012).

[5] G. Trambly de Laissardière, D. Mayou, and L. Magaud, Phys. Rev. B **86**, 125413 (2012).

[6] A. V. Rozhkov, A. O. Sboychakov, A. L. Rakhmanov, and F. Nori, Phys. Rep. **648**, 1 (2016).

[7] Y. Cao, V. Fatemi, S. Fang, K. Watanabe, T. Taniguchi, E. Kaxiras, and P. Jarillo-Herrero, Nature (London) **556**, 43 (2018).

[8] Y. Cao, V. Fatemi, A. Demir, S. Fang, S. L. Tomarken, J. Y. Luo, J. D. Sanchez-Yamagishi, K. Watanabe, T. Taniguchi, E. Kaxiras *et al.*, Nature (London) **556**, 80 (2018).

[9] Y. Xie, B. Lian, B. Jäck, X. Liu, C.-L. Chiu, K. Watanabe, T. Taniguchi, B. A. Bernevig, and A. Yazdani, Nature (London) **572**, 101 (2019).

[10] X. Lu, P. Stepanov, W. Yang, M. Xie, M. A. Aamir, I. Das, C. Urgell, K. Watanabe, T. Taniguchi, G. Zhang *et al.*, Nature (London) **574**, 653 (2019).

[11] A. Kerelsky, L. J. McGilly, D. M. Kennes, L. Xian, M. Yankowitz, S. Chen, K. Watanabe, T. Taniguchi, J. Hone, C. Dean *et al.*, Nature (London) **572**, 95 (2019).

[12] Y. Da Liao, Z. Y. Meng, and X. Y. Xu, Phys. Rev. Lett. **123**, 157601 (2019).

[13] M. Yankowitz, S. Chen, H. Polshyn, Y. Zhang, K. Watanabe, T. Taniguchi, D. Graf, A. F. Young, and C. R. Dean, Science **363**, 1059 (2019).

[14] S. L. Tomarken, Y. Cao, A. Demir, K. Watanabe, T. Taniguchi, P. Jarillo-Herrero, and R. C. Ashoori, Phys. Rev. Lett. **123**, 046601 (2019).

[15] Y. Cao, D. Chowdhury, D. Rodan-Legrain, O. Rubies-Bigorda, K. Watanabe, T. Taniguchi, T. Senthil, and P. Jarillo-Herrero, Phys. Rev. Lett. **124**, 076801 (2020).

[16] K. P. Nuckolls, M. Oh, D. Wong, B. Lian, K. Watanabe, T. Taniguchi, B. A. Bernevig, and A. Yazdani, Nature (London) **588**, 610 (2020).

[17] T. Soejima, D. E. Parker, N. Bultinck, J. Hauschild, and M. P. Zaletel, Phys. Rev. B **102**, 205111 (2020).

[18] S. Chatterjee, M. Ippoliti, and M. P. Zaletel, Phys. Rev. B **106**, 035421 (2022).

[19] E. Khalaf, N. Bultinck, A. Vishwanath, and M. P. Zaletel, arXiv:2009.14827.

[20] M. Xie and A. H. MacDonald, Phys. Rev. Lett. **124**, 097601 (2020).

[21] E. Khalaf, S. Chatterjee, N. Bultinck, M. P. Zaletel, and A. Vishwanath, Sci. Adv. **7**, eabf5299 (2021).

[22] A. T. Pierce, Y. Xie, J. M. Park, E. Khalaf, S. H. Lee, Y. Cao, D. E. Parker, P. R. Forrester, S. Chen, K. Watanabe *et al.*, Nat. Phys. **17**, 1210 (2021).

[23] Y.-D. Liao, X.-Y. Xu, Z.-Y. Meng, and J. Kang, Chin. Phys. B **30**, 017305 (2021).

[24] A. Rozen, J. M. Park, U. Zondiner, Y. Cao, D. Rodan-Legrain, T. Taniguchi, K. Watanabe, Y. Oreg, A. Stern, E. Berg *et al.*, Nature (London) **592**, 214 (2021).

[25] U. Zondiner, A. Rozen, D. Rodan-Legrain, Y. Cao, R. Queiroz, T. Taniguchi, K. Watanabe, Y. Oreg, F. von Oppen, A. Stern *et al.*, Nature (London) **582**, 203 (2020).

[26] Y. Saito, F. Yang, J. Ge, X. Liu, T. Taniguchi, K. Watanabe, J. Li, E. Berg, and A. F. Young, Nature (London) **592**, 220 (2021).

[27] J. M. Park, Y. Cao, K. Watanabe, T. Taniguchi, and P. Jarillo-Herrero, Nature (London) **592**, 43 (2021).

[28] Y. H. Kwan, Y. Hu, S. H. Simon, and S. A. Parameswaran, Phys. Rev. Lett. **126**, 137601 (2021).

[29] Y. D. Liao, J. Kang, C. N. Breiø, X. Y. Xu, H.-Q. Wu, B. M. Andersen, R. M. Fernandes, and Z. Y. Meng, Phys. Rev. X **11**, 011014 (2021).

[30] J. Kang, B. A. Bernevig, and O. Vafek, Phys. Rev. Lett. **127**, 266402 (2021).

[31] J. Liu and X. Dai, Phys. Rev. B **103**, 035427 (2021).

[32] F. Schindler, O. Vafek, and B. A. Bernevig, Phys. Rev. B **105**, 155135 (2022).

[33] E. Brillaux, D. Carpentier, A. A. Fedorenko, and L. Savary, Phys. Rev. Res. **4**, 033168 (2022).

[34] Z.-D. Song and B. A. Bernevig, Phys. Rev. Lett. **129**, 047601 (2022).

[35] J.-X. Lin, Y.-H. Zhang, E. Morissette, Z. Wang, S. Liu, D. Rhodes, K. Watanabe, T. Taniguchi, J. Hone, and J. Li, Science **375**, 437 (2022).

[36] S. Bhowmik, B. Ghawri, N. Leconte, S. Appalakondaiah, M. Pandey, P. S. Mahapatra, D. Lee, K. Watanabe, T. Taniguchi, J. Jung *et al.*, Nat. Phys. **18**, 639 (2022).

[37] T. Huang, X. Tu, C. Shen, B. Zheng, J. Wang, H. Wang, K. Khaliji, S. H. Park, Z. Liu, T. Yang *et al.*, Nature (London) **605**, 63 (2022).

[38] S. Zhang, X. Lu, and J. Liu, Phys. Rev. Lett. **128**, 247402 (2022).

[39] J. Herzog-Arbeitman, A. Chew, D. K. Efetov, and B. A. Bernevig, Phys. Rev. Lett. **129**, 076401 (2022).

[40] E. Y. Andrei and A. H. MacDonald, Nat. Mater. **19**, 1265 (2020).

[41] P. Stepanov, M. Xie, T. Taniguchi, K. Watanabe, X. Lu, A. H. MacDonald, B. A. Bernevig, and D. K. Efetov, Phys. Rev. Lett. **127**, 197701 (2021).

[42] H. C. Po, L. Zou, A. Vishwanath, and T. Senthil, Phys. Rev. X **8**, 031089 (2018).

[43] M. Koshino, N. F. Q. Yuan, T. Koretsune, M. Ochi, K. Kuroki, and L. Fu, Phys. Rev. X **8**, 031087 (2018).

[44] J. Kang and O. Vafek, Phys. Rev. X **8**, 031088 (2018).

[45] H. C. Po, H. Watanabe, and A. Vishwanath, Phys. Rev. Lett. **121**, 126402 (2018).

[46] H. C. Po, L. Zou, T. Senthil, and A. Vishwanath, Phys. Rev. B **99**, 195455 (2019).

[47] S. Liu, E. Khalaf, J. Y. Lee, and A. Vishwanath, Phys. Rev. Res. **3**, 013033 (2021).

[48] Y. Zhang, K. Jiang, Z. Wang, and F. Zhang, Phys. Rev. B **102**, 035136 (2020).

[49] B. A. Bernevig, Z.-D. Song, N. Regnault, and B. Lian, Phys. Rev. B **103**, 205413 (2021).

[50] B. Lian, Z.-D. Song, N. Regnault, D. K. Efetov, A. Yazdani, and B. A. Bernevig, Phys. Rev. B **103**, 205414 (2021).

[51] B. A. Bernevig, B. Lian, A. Cowsik, F. Xie, N. Regnault, and Z.-D. Song, Phys. Rev. B **103**, 205415 (2021).

[52] N. Bultinck, E. Khalaf, S. Liu, S. Chatterjee, A. Vishwanath, and M. P. Zaletel, Phys. Rev. X **10**, 031034 (2020).

[53] O. Vafek and J. Kang, Phys. Rev. Lett. **125**, 257602 (2020).
[54] X. Zhang, G. Pan, Y. Zhang, J. Kang, and Z. Y. Meng, Chin. Phys. Lett. **38**, 077305 (2021).
[55] J. S. Hofmann, E. Khalaf, A. Vishwanath, E. Berg, and J. Y. Lee, Phys. Rev. X **12**, 011061 (2022).
[56] G. Pan, X. Zhang, H. Li, K. Sun, and Z. Y. Meng, Phys. Rev. B **105**, L121110 (2022).
[57] Y. Ouyang and X. Y. Xu, Phys. Rev. B **104**, L241104 (2021).
[58] X. Zhang, G. Pan, X. Y. Xu, and Z. Y. Meng, Phys. Rev. B **106**, 035121 (2022).
[59] G. Pan, X. Zhang, H. Lu, H. Li, B.-B. Chen, K. Sun, and Z. Y. Meng, Phys. Rev. Lett. **130**, 016401 (2023).
[60] B. Lian, Z. Wang, and B. A. Bernevig, Phys. Rev. Lett. **122**, 257002 (2019).
[61] J. González and T. Stauber, Phys. Rev. Lett. **122**, 026801 (2019).
[62] S. Raghu, X.-L. Qi, C. Honerkamp, and S.-C. Zhang, Phys. Rev. Lett. **100**, 156401 (2008).
[63] B.-B. Chen, Y. D. Liao, Z. Chen, O. Vafek, J. Kang, W. Li, and Z. Y. Meng, Nat. Commun. **12**, 5480 (2021).
[64] X. Lin, B.-B. Chen, W. Li, Z. Y. Meng, and T. Shi, Phys. Rev. Lett. **128**, 157201 (2022).
[65] C. Shen, Y. Chu, Q. Wu, N. Li, S. Wang, Y. Zhao, J. Tang, J. Liu, J. Tian, K. Watanabe, T. Taniguchi, R. Yang, Z. Y. Meng, D. Shi, O. V. Yazyev, and G. Zhang, Nat. Phys. **16**, 520 (2020).
[66] X. Liu, C.-L. Chiu, J. Y. Lee, G. Farahi, K. Watanabe, T. Taniguchi, A. Vishwanath, and A. Yazdani, Nat. Commun. **12**, 2732 (2021).
[67] M. Huang, Z. Wu, J. Hu, X. Cai, E. Li, L. An, X. Feng, Z. Ye, N. Lin, K. T. Law *et al.*, Natl. Sci. Rev. **10**, nwac232 (2022).
[68] B. A. Bernevig, Z.-D. Song, N. Regnault, and B. Lian, Phys. Rev. B **103**, 205411 (2021).
[69] Y. Ge and A. Y. Liu, Phys. Rev. B **87**, 241408(R) (2013).
[70] R. Roldán, E. Cappelluti, and F. Guinea, Phys. Rev. B **88**, 054515 (2013).
[71] N. F. Q. Yuan, K. F. Mak, and K. T. Law, Phys. Rev. Lett. **113**, 097001 (2014).
[72] X. Zhang, K. Sun, H. Li, G. Pan, and Z. Y. Meng, Phys. Rev. B **106**, 184517 (2022).
[73] L. An, X. Cai, D. Pei, M. Huang, Z. Wu, Z. Zhou, J. Lin, Z. Ying, Z. Ye, X. Feng, R. Gao, C. Cacho, M. Watson, Y. Chen, and N. Wang, Nanoscale Horiz. **5**, 1309 (2020).
[74] See Supplemental Material at http://link.aps.org/supplemental/10.1103/PhysRevB.107.L241105 for the detailed QMC implementation of the model, the analyses of the polynomial sign behavior, excitations from exact solution, and supplemental figures.
[75] M. Troyer and U.-J. Wiese, Phys. Rev. Lett. **94**, 170201 (2005).
[76] G. Pan and Z. Y. Meng, arXiv:2204.08777.
[77] C. L. Henley, Phys. Rev. Lett. **62**, 2056 (1989).
[78] F. Xie, J. Kang, B. A. Bernevig, O. Vafek, and N. Regnault, Phys. Rev. B **107**, 075156 (2023).
[79] A. W. Sandvik, Phys. Rev. B **57**, 10287 (1998).
[80] K. Beach, arXiv:cond-mat/0403055.
[81] A. W. Sandvik, Phys. Rev. E **94**, 063308 (2016).
[82] O. F. Syljuåsen, Phys. Rev. B **78**, 174429 (2008).
[83] G.-Y. Sun, Y.-C. Wang, C. Fang, Y. Qi, M. Cheng, and Z. Y. Meng, Phys. Rev. Lett. **121**, 077201 (2018).
[84] N. Ma, G.-Y. Sun, Y.-Z. You, C. Xu, A. Vishwanath, A. W. Sandvik, and Z. Y. Meng, Phys. Rev. B **98**, 174421 (2018).
[85] Y.-C. Wang, M. Cheng, W. Witczak-Krempa, and Z. Y. Meng, Nat. Commun. **12**, 5347 (2021).
[86] W. Jiang, Y. Liu, A. Klein, Y. Wang, K. Sun, A. V. Chubukov, and Z. Y. Meng, Nat. Commun. **13**, 2655 (2022).
[87] C. Zhou, M.-Y. Li, Z. Yan, P. Ye, and Z. Y. Meng, Phys. Rev. Res. **4**, 033111 (2022).
[88] H. Shao, Y. Q. Qin, S. Capponi, S. Chesi, Z. Y. Meng, and A. W. Sandvik, Phys. Rev. X **7**, 041072 (2017).
[89] C. Zhou, Z. Yan, H.-Q. Wu, K. Sun, O. A. Starykh, and Z. Y. Meng, Phys. Rev. Lett. **126**, 227201 (2021).
[90] H. Li, Y. D. Liao, B.-B. Chen, X.-T. Zeng, X.-L. Sheng, Y. Qi, Z. Y. Meng, and W. Li, Nat. Commun. **11**, 1111 (2020).
[91] Z. Hu, Z. Ma, Y.-D. Liao, H. Li, C. Ma, Y. Cui, Y. Shangguan, Z. Huang, Y. Qi, W. Li, Z. Y. Meng, J. Wen, and W. Yu, Nat. Commun. **11**, 5631 (2020).